DOI 10.1007/s10812-017-0497-0
Journal of Applied Spectroscopy, Vol. 84, No. 3, July, 2017 (Russian Original Vol. 84, No. 3, May–June, 2017)

ESTIMATION OF LATTICE STRAIN IN ZnO NANOPARTICLES PRODUCED BY LASER ABLATION AT DIFFERENT TEMPERATURES

E. Solati and D. Dorranian* UDC 620.3;548.0;546.47

The effects of water temperature on the characteristics of ZnO nanoparticles produced by laser ablation method in water were investigated experimentally. The nanoparticles were prepared by pulsed laser ablation of a zinc metal target in distilled water at different temperatures. The synthesized ZnO nanoparticles were characterized using X-ray diffraction analysis and transmission electron microscopy. The results show that the produced samples are crystalline with a hexagonal wurtzite phase. Transmission electron microscopy has revealed that the ZnO nanoparticles are spherical. The strain and the crystallite size of the nanoparticles were investigated by X-ray peak broadening. The mean crystallite size of the ZnO nanoparticles estimated from the TEM images is in good agreement with three models of the Williamson–Hall method. According to the results, the size distribution of the produced ZnO nanoparticles depends strongly on the temperature of the ablation environment.

Keywords: *ZnO nanoparticles, laser ablation, crystal structure, lattice strain.*

Introduction. Zinc oxide is attracting extraordinary attention due to its promising properties such as having a wide direct band gap of 3.37 eV and very high excitonic binding energy of 60 meV at room temperature [1]. Furthermore, it is well known that low-dimensional structures may have superior optical properties over bulk material due to the quantum confinement effect [2].Therefore, the controlled synthesis of various ZnO nanostructures, such as nanocrystals, nanowires, nanobelts, and other complex nanoarchitectures, has been extensively explored [3].

A wide variety of techniques have been exploited to fabricate ZnO nanostructures. Among different preparation methods for producing nanoparticles, the laser ablation technique has been successfully developed [4, 5]. Pulsed laser ablation (PLA) in liquid media is a quick, easy, one-step, and rapidly emerging approach for physical synthesis of colloidal solution of nanoparticles. In PLA process in liquid media, strong reactions may take place between the ablated species and encountered solution molecules; thus, the nanocrystals can be prepared after rapid reactive quenching in liquid [6, 7]. In this process the laser parameters such as laser frequency, laser pulse energy, and laser wavelength as well as the laser–solid interaction are important processing factors by which the characteristics of produced nanoparticles may be controlled [6, 8–11].

In this work we have focused on the crystalline structure of produced nanoparticles. A perfect crystal is one that contains no point, linear, or planar imperfections. But there are a wide variety of crystallographic defects. This deviation from perfect crystallinity is the reason for broadening the X-ray diffraction peaks of materials. Crystallite size and lattice strain are two main properties extracted from peak broadening analysis. Lattice strain is a measure of the distribution of lattice constants arising from crystal imperfections, such as lattice dislocation. There are other sources of strain, which are the grain boundary triple junction, coherency stresses, contact or sinter stresses, stacking faults, etc. [12–15].

There are several published works on estimation of lattice strain in ZnO nanoparticles. Zak et al. published their results on the X-ray analysis of ZnO nanoparticles produced by a sol-gel combustion method [12]. Mote et al. estimated the lattice strain in nanometer-sized ZnO particles synthesized by a coprecipitation method [13]. Bindu and Thomas reported the characterization of ZnO nanoparticles synthesized from chitosan and zinc chloride by a precipitation method [14]. In 2009 ZnO nanoparticles were synthesized by a hydrothermal process and characterized by X-ray diffraction and transmission electron microscopy [15].

*To whom correspondence should be addressed.

Plasma Physics Research Center, Science and Research Branch, Islamic Azad University, Tehran, Iran; e-mail: doran@srbiau.ac.ir; d.dorranian@gmail.com. Published in Zhurnal Prikladnoi Spektroskopii, Vol. 84, No. 3, pp. 475–482, May–June, 2017. Original article submitted October 27, 2015.

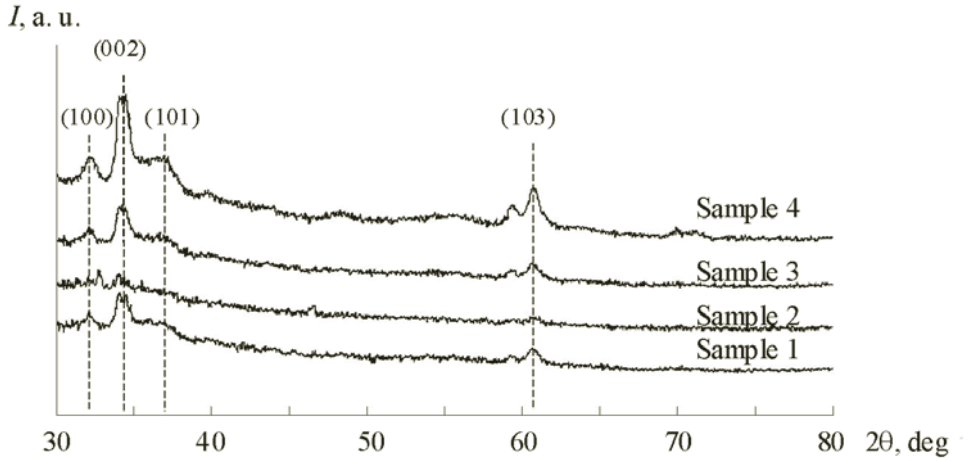

Fig. 1. X-ray diffraction pattern of ZnO nanoparticles.

In this paper we present the experimental results of the effects of water temperature on the lattice structure and lattice strain and stress of ZnO nanoparticles produced via laser ablation in distilled water.

Experimental. ZnO nanoparticles were produced by PLA of a zinc plate (99.9%) in distilled water. The Zn metal plate was placed on the bottom of an open glass cylindrical vessel filled with 20 mL of distilled water. Height of water on the zinc plate was 8 mm. The target was cleaned ultrasonically in alcohol, acetone, and deionized water before the experiments. The plate was irradiated with a pulsed Nd:YAG laser operating at 10 Hz repetition rate of 7 ns pulse width with 500 laser pulses at 0.7 J/cm^2 fluence. The laser beam was 6 mm in diameter before the lens and was focused on the target surface using a 80 mm focal length lens. The spot size of the laser beam on the target surface was calculated to be 50 μm. To study the effect of ablation environment temperature, the ablation contain was placed on an automatic heater, and the temperature of the water was controlled by a thermometer. Samples 1–4 were produced in water at 0, 20, 40, and 60^{o}C temperature respectively, which are labeled as s1 to s4 in this report.

X-ray diffraction pattern (XRD) was measured employing an X-PERTPRO MPD X-ray diffractometer from the PANalitical, and transmission electron microscopy (TEM) was carried out using a Zeiss EM10C.

Results and Discussion. *XRD studies of ZnO nanoparticles.* Figure 1 shows an XRD pattern of the as-prepared nanoparticles. The suspensions were dropped on a copper foil and dried at room temperature for the XRD measurement. The XRD spectrum shows the multistructure of the ZnO nanoparticles and that the intensity of peaks is changed for the nanoparticles synthesized at different temperatures. The intensity of XRD peaks is decreased from s1 to s2, while from s2 to s4 the intensity of peaks is increased. The increase in the intensity of XRD peaks is due to increasing crystallinity of the samples. From the XRD patterns it can be seen that the ZnO nanoparticles synthesized at 20^{o}C have mainly amorphous structure rather than crystalline. The effect of temperature on formation of the nanoparticles can be attributed to an increase in surface mobility of arriving atoms. There are more disordered structures in the ZnO nanoparticles that were formed in the low temperature condition than in other samples. To explain the properties of the nanoparticles generated at 0^{o}C, the unique characteristics of water at 0 to 4^{o}C must be taken into account.

The XRD peaks of the nanoparticles occurred at very similar angles, and most of them are different with Zn target peaks. It can be concluded that Zn and O atoms are formed during the ablation process. Ablation of atoms takes place and nucleation occurres during the plasma plume expansion phase on the target surface. The XRD pattern of the ZnO nanoparticles in water at different temperature reveals that they possess the hexagonal wurtzite structure. Results are in good agreement with other reports, which are mostly on the production of the ZnO nanoparticles by laser ablation in water [9].

Determination of crystallite size and lattice constants. The average crystallite size of the nanoparticle D of ZnO generated by laser ablation was estimated using the standard known as the Scherrer formula [16]:

$$D = k\lambda/\beta \cos\theta\,, \qquad (1)$$

where k is a constant ($0.89 < k < 1$), λ is wavelength of the X-ray, β is the FWHM (full width at half maximum) of the diffraction peak, and θ is the diffraction angle. In this work, the intensity of peak (002) plane is much stronger than that of the other peaks. This indicates that the ZnO nanocrystals have a preferential crystallographic (002) orientation. In Fig. 2, cos θ is

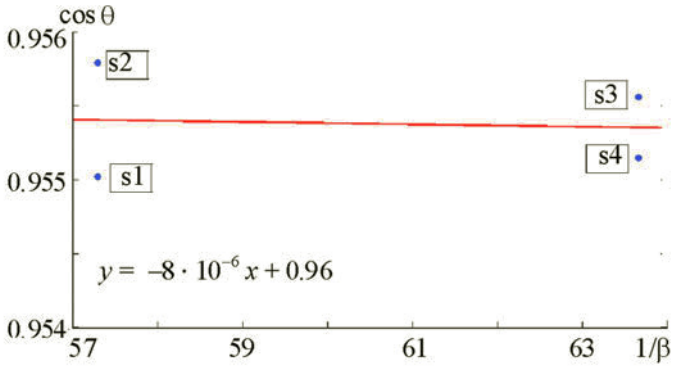

Fig. 2. Scherrer plot of the ZnO nanoparticles synthesized at different temperature. The average crystall size is extracted from the slope of the fit line.

TABLE 1. Lattice Parameters of Different Samples

Sample	a, Å	c, Å
s1	3.2188	5.1952
s2	3.2149	5.2394
s3	3.2081	5.2095
s4	3.1975	5.2260

ploted versus 1/β for the ZnO nanoparticles synthesized at different environment temperatures for (002) peak. The average crystallite size was extracted from the fit line slope. The peaks of the X-ray diffraction pattern of s2 have low intensity and large width. The low intensity of diffracted X-ray photons from the ZnO nanoparticles in this sample confirms that the structure of the nanoparticles tends to an amorphous type, and the large width of the peak confirms that the crystallite size of the nanoparticles in this sample is small. Adhesion of the ZnO nanoparticles with increasing water temperature leads to increase in the grain size of the samples.

There are two lattice constants for a hexagonal unit cell, known as a and c which can be calculated from XRD spectrum of samples using the following equation [17]:

$$1/d^2 = (4/3)[(h^2 + k^2 + hk)/a^2] + l^2/c^2 , \quad (2)$$

where h, k, and l are known as the Miller indices. According to the Bragg equation, the lattice constant a for the (100) plane is calculated by

$$a = \lambda/\sqrt{3}\sin\theta \quad (3)$$

and for the (002) plane, the lattice constant c is calculated by

$$c = \lambda/\sin\theta . \quad (4)$$

where a decreases with increasing temperature while c changes randomly. Lattice constants of the unit cell for these planes are presented in Table 1. The salient feature in the present ZnO nanoparticles is a drop of small magnitude in the lattice parameter a with increasing environment temperature. In this case, increasing the environment temperature will increase plasma pressure during the laser ablation. This leads to an overall reduction in atomic vibrations, so a decreases with increasing temperature, but because the plasma is cooled in a short time, c is not changed uniformly by increasing plasma pressure [9]. The results show that the lattice parameters a and c depend on environment temperature in laser ablation in linear and nonlinear ways, respectively. The lattice parameter for the c axis changes more rapidly with temperature than that of the a axis. This can be attributed to the preferential accommodation of the solutes along either the c or a axis [18].

In the ZnO nanoparticles synthesized at 20 to 60°C, it is observed that the position of the (002) diffraction peak shifts towards the higher angles. This can be a result of the release of intrinsic strain during the laser ablation process. It shows the relaxation of the crystal lattice structure and reduction of the nanoparticles surface energy.

TABLE 2. Geometric Parameters for Synthesized ZnO Nanoparticles

Sample	Scherrer method	Williamson–Hall methods									TEM
		UDM		USDM			UDEDM				
	D, nm	D, nm	$\varepsilon \times 10^{-3}$	D, nm	σ, MPa	$\varepsilon \times 10^{-3}$	D, nm	u, kJ/m^3	σ, MPa	$\varepsilon \times 10^{-3}$	D, nm
s1	9.24	8.35	3.5764	8.73	363	2.8525	8.55	64.74	128	1.0078	9.84
s2	9.23	10.33	2.2149	11.01	188	1.4773	10.70	20.78	72	0.5669	10.69
s3	10.26	8.17	3.8625	8.58	390	3.0646	8.39	74.96	137	1.0787	9.80
s4	10.26	6.39	6.6414	6.83	646	5.0606	6.62	205.66	228	1.7952	6.55

Williamson–Hall methods. The strain induced in the ZnO nanoparticles due to crystal imperfection and distortion was calculated using the formula

$$\varepsilon = \beta/4 \tan\theta. \tag{5}$$

Williamson and Hall [15] proposed a method of deconvoluting size and strain broadening by looking at the peak width as a function of diffraction angle 2θ. They obtained the mathematical expressions

$$\beta = \beta_D + \beta_S, \tag{6}$$

$$\beta_{hkl} = k\lambda/D \cos\theta + 4\varepsilon \tan\theta. \tag{7}$$

By rearranging the above equation, we get

$$\beta_{hkl} \cos\theta = k\lambda/D + 4\varepsilon \sin\theta. \tag{8}$$

This equation is the Williamson–Hall equation, which represents the uniform deformation model (UDM), where the strain is assumed to be uniform in all crystallographic directions [13]. In Fig. 3 the UDM results, i.e., $\beta_{hkl} \cos\theta$, was plotted versus 4 sin θ for the peaks of the ZnO nanoparticles. From the linear fit to the data, the crystallite size D was extracted from the y-intercept, and the strain ε was extracted from the fitted line slope. The plots show a negative strain for the ZnO nanoparticles. With increasing environment temperature of the laser ablation, the slope of the fit is increased. This may be due to decreasing lattice parameter a, which was observed in the lattice parameter calculation. The estimated values of the strain and the crystallite size by the UDM model are presented in Table 2.

In the uniform stress deformation model (USDM), the generalized Hooke's law refers to the strain, keeping only the linear proportionality between the stress and strain as given by $\sigma = Y\varepsilon$, where σ is the stress of the crystal and Y is the modulus of elasticity or Young's modulus [12–15, 19]. In the USDM model, the lattice deformation stress is assumed to be uniform in all crystallographic directions, and a small strain is assumed to be present in the particles [14]. In this approach, the Williamson–Hall equation is modified by substituting the value of ε in Eq. (8):

$$\beta_{hkl} \cos\theta = k\lambda/D + 4\sigma \sin\theta/Y_{hkl}. \tag{9}$$

For the ZnO nanoparticles with a hexagonal crystal phase, Young's modulus is given by the following relation [20]:

$$Y_{hkl} = \frac{[h^2 + (h + 2k)^2/3 + (al/c)^2]^2}{s_{11}[h^2 + (h + 2k)^2/3]^2 + s_{33}(al/c)^4 + (2s_{13} + s_{44})[h^2 + (h + 2k)^2/3](al/c)^2}, \tag{10}$$

where a and c are lattice parameters and s_{11}, s_{13}, s_{33}, and s_{44} are elastic compliances of ZnO. Their values are 7.858×10^{-12}, -2.206×10^{-12}, 6.940×10^{-12}, and 23.57×10^{-12} m^2/N, respectively [21].Young's modulus for the preferred orientation peak of the ZnO nanoparticles was calculated as ~127 GPa. Plots are drawn by taking 4 sin θ/Y and $\beta_{hkl} \cos\theta$ along x and y axis, respectively, for the ZnO nanoparticles synthesized at different temperatures, as shown in Fig. 4. The lattice deformation stress and crystallite size of the ZnO nanoparticles were extracted from the slope and intersection of the linear fit made to the plot. As can be seen, the stress calculated from the slope of the fitted line increases with increasing environment temperature for the ZnO nanoparticles synthesized at 20 to 60°C. The estimated values of the stress, strain and the crystallite size by the USDM model are presented in Table 2.

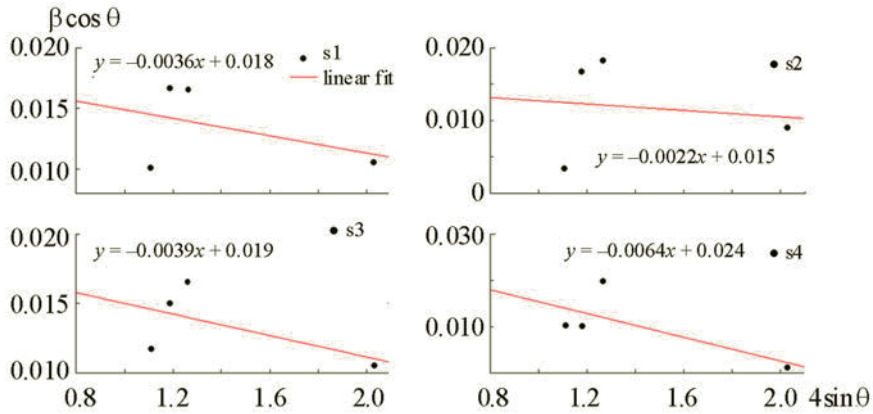

Fig. 3. The Williamson–Hall analysis of the ZnO nanoparticles synthesized at different temperature assuming UDM.

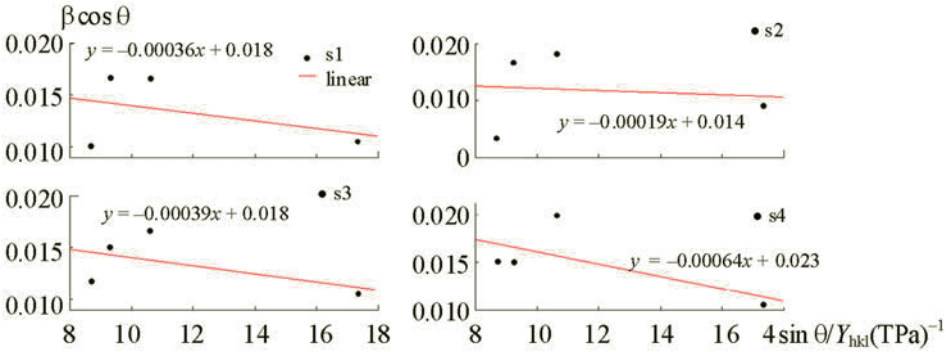

Fig. 4. The modified form of Williamson–Hall analysis assuming USDM for the ZnO nanoparticles synthesized at different temperature.

According Eq. (8), we have considered uniform and homogeneous strain in all crystallographic directions. But, in many cases, the assumption of homogeneity and isotropy is not satisfied. Furthermore, the constants of proportionality associated with the stress–strain relation are no longer independent when the strain energy density u is considered [15]. So, there is another model that can be used to determine the energy density of a crystal called the uniform deformation energy density model (UDEDM). According to Hooke's law, the energy density u (energy per unit volume) can be calculated from $u = (\varepsilon^2 Y_{hkl})/2$ [12]. By substituting $\sigma/Y = \varepsilon$ in the equation for u, one obtains $u = \sigma^2/(2Y_{hkl})$. In this model, the Williamson–Hall equation is modified by substituting the energy density in Eq. (9):

$$\beta_{hkl} \cos\theta = k\lambda/D + (4 \sin\theta(2u/Y_{hkl})^{1/2}) \,. \tag{11}$$

A plot of ($\beta_{hkl} \cos\theta$) versus ($4 \sin\theta(2/Y_{hkl})^{1/2}$) is presented in Fig. 5. From the slope of the linear fit to the data, the energy density u was calculated and the crystallite size D was extracted from the y-intercept. The estimated values of the energy density, stress, strain, and the crystallite size by the UDEDM model are presented in Table 2. The results of these plots show a change in energy density of the ZnO nanoparticles synthesized at different environment temperatures. In this experiment the energy density of the ZnO nanoparticles increased with increasing environment temperature for the nanoparticles synthesized at 20 to 60°C. The salient feature in the UDEDM model is the smaller values of the stress and strain in comparison with the other models.

A comparison of the three models for investigation of nanocrystalline properties of the ZnO nanoparticles is possible from the analysis of Figs. 3–5. The scattering of the data points away from the linear expression is less in Fig. 4 compared with Figs. 3 and 5. The average crystallite size and the strain values obtained from the UDM, UDSM, and UDEDM models were found to be accurate, comparable, and reasonable, as in the plots of these models their data points lay close to the linear

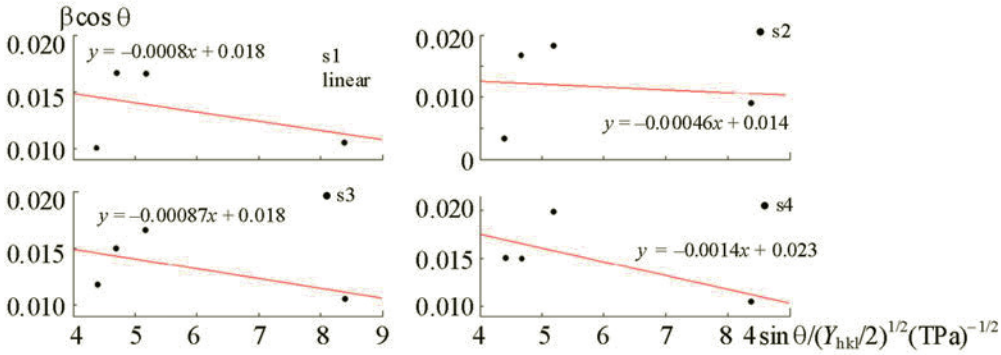

Fig. 5. The modified form of Williamson–Hall analysis assuming UDEDM for the ZnO nanoparticles synthesized at different temperature.

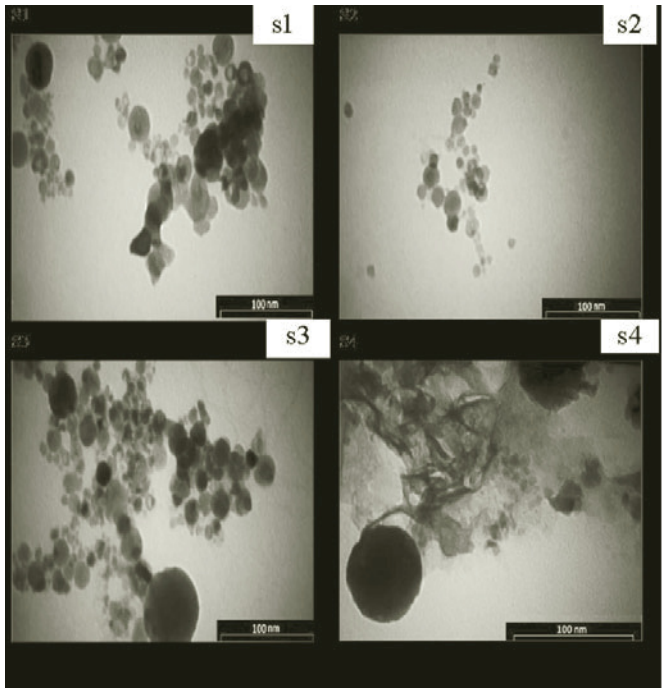

Fig. 6. TEM micrographs of ZnO nanoparticles.

fit. In this work, the values of the average crystallite size of the ZnO nanoparticles synthesized at different environment temperatures, obtained from the UDM, USDM, and UDEDM models, are approximately similar. This signifies that the inclusion of strain in different forms has a very small effect on the average crystallite size of the ZnO nanoparticles. The difference in crystallite size obtained from the Scherrer formula and Williamson–Hall methods is large. This is because of the large difference in the average particle size distribution [15].

TEM studies of ZnO nanoparticles. TEM micrographs of the nanoparticles in the scale of 100 nm are displayed in Fig. 6. Figure 7 also shows the size distribution of the ZnO nanoparticles. The products are composed of particles with nearly spherical shape. This morphology of nanoparticles was reported by Zeng et al. [22]. The particle sizes and size distribution are dependent on the environment temperature. As can be seen, the size of the nanoparticles increases from s1 to s2 and then decreases with increasing water temperature. Similar results can be observed in the UDM, USDM, and UDEDM models. The existence of nonuniform strain in some of the particles can be seen in the TEM micrographs. The average size of the ZnO nanoparticles obtained by the TEM micrographs is presented in Table 2.

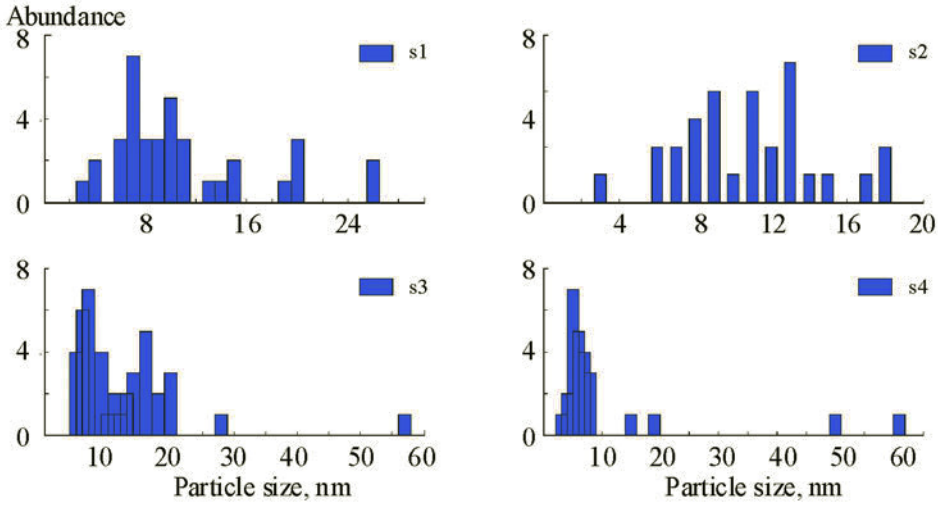

Fig. 7. Size distribution of ZnO nanoparticles, extracted from TEM images.

Conclusions. We have synthesized ZnO nanoparticles by pulsed laser ablation of a zinc metal target in distilled water at different temperatures. The effects of the environment temperature on the nanostructure and morphology of the ZnO nanoparticles have been investigated. XRD data reveal that these nanoparticles possess the hexagonal wurtzite structure. Line broadening of the ZnO nanoparticles was due to the small crystallite size and lattice strain. From the results, it was observed that the strain value increased, but the particle size decreased, as the environment temperature was increased from 20 to 60^{o}C, and this event is reversed when increasing the environment temperature from 0 to 20^{o}C. To explain the properties of the nanoparticles generated at 0^{o}C, the unique characteristics of water at 0 to 4^{o}C can be taken into account. The difference between the extracted crystallite size from the Scherrer equation and TEM micrographs is rather high, while the extracted crystalline size from the Williamson–Hall equation is in good agreement with the TEM micrographs. Therefore, the Williamson–Hall methods result in a more accurate estimation of the crystallite size compared to the Scherrer equation. From the TEM micrographs results, the ZnO nanoparticles are almost spherical, and the particle sizes and size distribution are strongly dependent on the ablation environment temperature.

REFERENCES

1. C. Y. Lee, Y. T. Haung, W. F. Su, and C. F. Lin, *Appl. Phys. Lett.*, **89**, 231116 (2006).
2. Y. Gong, T. Andelman, G. F. Neumark, S. O'Brien, and I. L. Kuskovsky, *Nanoscale Res. Lett.*, **2**, 297–302 (2007).
3. H. Zeng, Z. Li, W. Cai, B. Cao, P. Liu, and S. Yang, *J. Phys. Chem. B*, **111**, 14311–14317 (2007).
4. A. Abdolvand, S. Z. Khan, Y. Yuan, P. L. Crouse, M. J. J. Schmidt, M. Sharp, Z. Liu, and L. Li, *Appl. Phys. A*, **91**, 365 (2008).
5. V. Amendola and M. Meneghetti, *Phys. Chem. Chem. Phys.*, **11**, 3805 (2009).
6. D. Dorranian, E. Solati, and L. Dejam, *Appl. Phys. A.*, **109**, 307–314 (2012).
7. S. C. Singh and R. Gopal, *Appl. Surf. Sci.*, **258**, 2211–2218 (2012).
8. E. Solati, M. Mashayekh, and D. Dorranian, *Appl. Phys. A*, **112**, 689–694 (2013).
9. E. Solati, L. Dejam, and D. Dorranian, *Opt. Laser Technol.*, **58**, 26–32 (2014).
10. E. Solati and D. Dorranian, *J. Clust. Sci.*, **26**, 727–742 (2015).
11. Ch. Zhao, Y. Huang, and J. T. Abiade, *Mater. Lett.*, **85**, 164–167 (2012).
12. A. Khorsand Zak, W. H. Abd. Majid, M. E. Abrishami, and R. Yousefi, *Solid State Sci.*, **13**, 251–256 (2011).
13. V. D. Mote, Y. Purushotham, and B. N. Dole, *J. Theor. Appl. Phys.*, **6**, 1–8 (2012).
14. P. Bindu and Sabu Thomas, *J. Theor. Appl. Phys.*, **8**, 1–12 (2014).
15. R. Yogamalar, R. Srinivasan, A. Vinu, K. Ariga, and A. Ch. Bose, *Solid State Commun.*, **149**, 1919–1923 (2009).
16. C. Suryanarayana and M. G. Norton, *X-Ray Diffraction a Practical Approach*, Plenum Press, New York (1998).
17. M. Tiemann, F. Marlow, J. Hartikainen, O. Weiss, and M. Linder, *J. Phys. Chem. C*, **112**, 1463–1467 (2008).

18. A. J. Saldivar-Garcia, and H. F. Lopez, *Metall. Mater. Trans. A*, **35**, 2517–2523 (2004).
19. K. Venkateswarlu, A. ChandraBose, and N. Rameshbabu, *Physica B*, **405**, 4256–4261 (2010).
20. J. Zhang, Y. Zhang, K.W. Xu, and V. Ji, *Solid State Commun.*, **139**, 87–91 (2006).
21. J. F. Nye, *Physical Properties of Crystals: Their Representation by Tensors and Matrices*, Oxford Science Publications, New York (1985).
22. H. Zeng, W. Cai, Y. Li, J. Hu, and P. Liu, *J. Phys. Chem. B*, **109**, 18260–18266 (2005).